Asian Journal of Chemistry; Vol. 37, No. 3 (2025), 661-672

ASIAN JOURNAL OF CHEMISTRY

https://doi.org/10.14233/ajchem.2025.33297

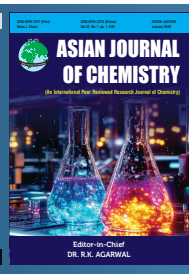

Lactobacillus sp., Mediated Synthesis of Zinc Oxide Nanoparticles and their Anticancer Activity on A549 Lung Cancer Cell Lines

M.I. ANJANA, M. ABIYOGA, K. RAJALAKSHMY and P. SARAVANA KUMARI*

Department of Microbiology, Rathnavel Subramaniam (RVS) College of Arts and Science, Coimbatore-641402, India

*Corresponding author: E-mail: sarankumaribs@gmail.com

Received: 30 December 2024; *Accepted*: 10 February 2025; *Published online*: 28 February 2025; AJC-21923

Targeting certain signaling pathways may enable innovative therapeutics to overcome chemotherapy and radiation's limitations, therefore, nanoparticle biosynthesis provides a promising alternative. This study investigates *Lactobacillus* sp., mediated zinc oxide nanoparticles (ZnO NPs) as a therapeutic approach against lung cancer A549 cells. The ZnO NPs were characterized using UV-Vis spectroscopy, FTIR, XRD, SEM, TEM, EDX, zeta potential and DLS analyses, confirming their nanoscale size and structural integrity. The UV-Vis spectra analysis of ZnO NPs revealed a significant absorption peak at approximately 392 nm. FTIR investigation confirms the functional groups in *Lactobacillus* sp., mediated ZnO NPs. Electron microscopy and XRD validated the spherical/cubic crystalline structure of ZnO NPs, averaging 30-40 nm in size. Strong signals in EDAX spectrum confirmed ZnO NPs formation. Zeta potential and DLS analysis showed biosynthesized ZnO NPs stability and particle size. The cytotoxic effect of ZnO NPs on A549 cancer cells was dose- and time-dependent, with an IC_{50} at 38 µg/mL. Morphological changes such as cell shrinkage and nuclear fragmentation in treated cell lines indicative of apoptosis observed *via* AO/EB staining. Flow cytometry revealed that ZnO NPs induced cell cycle arrest and apoptosis. Additionally, ZnO NPs significantly reduced A549 cell migration. These findings highlight the potential of *Lactobacillus* sp., mediated ZnO NPs as an eco-friendly, novel and effective strategy in cancer nanomedicine for lung cancer treatment.

Keywords: Biosynthesis, Drug delivery, *Lactobacillus* sp., Anticancer activity, A549 Cancer cell line.

INTRODUCTION

Human lung cancer is the most frequently diagnosed cancer and a leading cause of cancer-related deaths among humans worldwide, with over 2.48 million (12% among all cancer types) new cases reported annually and 1 out of 5 deaths from cancer (1.8 million deaths annually, that is 19% of the cancer deaths in worldwide) are due to lung cancer [1]. It is broadly categorized into two main types; non-small cell lung cancer (NSCLC), which makes up about 84% of cases and small cell lung cancer (SCLC) comprising approximately 13%. NSCLC often has a better prognosis compared to SCLC but still presents significant challenges in advanced stages [1,2]. Its incidence has risen significantly in the last three decades due to improved diagnostic methods, increased cancer registration and changes in risk factor profiles [3]. These molecular insights have led to personalized treatment approaches involving surgery, chemotherapy, radiotherapy, hormonal therapy and targeted biological therapies [3,4].

Nanoparticles represent a transformative approach to fight against lung cancer, offering targeted, efficient and minimally invasive treatment options. These nanoscale materials are engineered to deliver therapeutic agents specifically to cancer cells, improving efficacy while minimizing damage to healthy tissues [5]. Their small size, surface modifiability and unique physicochemical properties make them ideal for overcoming challenges associated with traditional therapies, such as chemoresistance, off-target effects and systemic toxicity [6]. For instance, nanoparticles can induce immunogenic cell death in cancer cells, enhancing the antitumor immune response and potentially preventing recurrence [7]. A variety of metal oxide nanoparticles have been synthesized, including titanium dioxide (TiO_2), silicon dioxide (SiO_2), nickel oxide (NiO), copper oxide (CuO), iron oxide (Fe_3O_4, Fe_2O_3) and zinc oxide (ZnO), employing various methods [8]. Each of these nanomaterials displays distinct morphologies, such as spherical, triangular, star and nanowire forms. With their numerous uses in the food industry,

medicine, energy and environment, these nanoparticles are gaining both commercial and scientific attention [9,10].

The synthesis of nanoparticles for lung cancer treatment typically involves methods like chemical reduction, sol-gel processing and green synthesis. These processes yield a range of nanomaterials, including metal-based nanoparticles (*e.g.* gold, zinc and silver), metal oxides, polymeric nanoparticles and liposomes. These nanoparticles can be loaded with anticancer drugs, ligands and imaging agents, enabling targeted therapy while minimizing adverse effects [11]. However, challenges such as scalability, reproducibility and regulatory hurdles remain critical in translating these technologies from research to clinical applications [12]. Studies highlight the potential of nanoparticle synthesis to overcome limitations in conventional lung cancer therapies including multidrug resistance and non-specific systemic distribution [13].

While zinc nanoparticles hold immense potential in diverse applications, ensuring their safe use requires careful control of their synthesis, dosage and environmental impact. Ongoing research focuses on optimizing their biocompatibility and developing eco-friendly production methods to maximize their benefits while minimizing risks [14]. Now-a-days, chemically synthesized zinc nanoparticles attributes in more toxic effect in pharmaceutical industry after a few days of treatment. Recently, in nanobiotechnology field, biosynthesis and use of nanoparticles considered as cost-effective and less toxic. Where, ZnO NPs have shown as promising with high binding affinity towards the cancer cells and inducing reactive oxygen species to cause apoptosis, especially in breast and lung cancer cells [15]. Their biocompatibility and targeted action reduce side effects compared to conventional therapies [10].

Bacteria mediated synthesis of zinc oxide nanoparticles (ZnO NPs) is an innovative approach in nanomedicine, particularly for cancer therapy. This eco-friendly, cost-effective method leverages bacterial enzymes and bioactive molecules to reduce zinc ions into ZnO NPs through extracellular or intracellular pathways [16]. ZnO NPs synthesized from bacteria are investigated for their ability to induce selective cytotoxicity in lung cancer cells, leveraging mechanisms like oxidative stress generation and apoptosis induction [7]. Advances in microbial synthesis enable precise control over nanoparticle size, morphology and functionality, enhancing their efficacy in drug delivery and photothermal applications. This sustainable approach aligns with the growing demand for greener and efficient biomedical technologies, marking a significant advancement in personalized cancer treatment [17].

The bacterial genus *Lactobacillus* widely recognized for its role in food fermentation, has emerged as a significant player in biotechnological and therapeutic applications [18]. These non-pathogenic, probiotic bacteria are integral to maintaining gut health, enhancing mucosal immunity and producing bioactive compounds [19]. Especially, *Lactobacillus* sp., are being investigated for their role in combating cancer [20]. Their ability to modulate host immune responses and produce metabolites with cytotoxic effects against tumor cells has positioned them as potential agents in cancer therapeutics [21]. This opens new avenues for integrating the strains of the genus *Lactobacillus* in innovative treatment strategies, including nanoparticle mediated therapies, where their metabolites act as stabilizing and reducing agents for nanoparticle synthesis [19]. The green synthesis method employs non-pathogenic bacterial species such as *Bacillus subtilis* and *Lactobacillus* sp., which produce enzymes, proteins and bioactive metabolites acting as reducing and capping agents. These mechanisms simplify nanoparticle production, offering enhanced biocompatibility, low toxicity and eco-friendliness [6].

EXPERIMENTAL

Lactic acid bacteria based ZnO NPs synthesis: A stock solution of 1 M Zn^{2+} was prepared by dissolving zinc acetate in deionized water. The Zn^{2+} solution underwent filtration before being introduced into the bacterial culture medium. From cow milk, lactic acid bacteria were isolated using de Man, Rogosa and Sharpe (MRS) medium. Isolated bacteria transferred to sterile MRS broth and incubated for 48 h at 37 ºC. By centrifuging the bacterial culture for 10 min at 10,000 rpm and 4 ºC, the supernatant was extracted. The supernatant was then mixed with zinc acetate solution in a 1:1 ratio and permitted to incubated in dark at 30 ºC for 24 h. After the incubation period, a distinct colour change indicated the formation of ZnO NPs. This approach employs the cell-free supernatant of *Lactobacillus* sp., to synthesize biogenic nanoparticles, where the biological components present in the supernatant serve as reducing and stabilizing agents.

Characterization: UV-Vis absorption spectroscopy used to investigate the optical properties of ZnO NPs at wavelengths between 200 and 600 nm (Hitachi U-2001-Tokyo, Japan). A Fourier Transform Infrared (FT-IR) absorption spectrometer used to analyze the functional groups found in the ZnO NPs. FE-SEM (Carl- ZEISS Sigma 500 VP, Sigma, Germany), EDAX (EDX, Bruker, Germany) and TEM (JEM-2100, JEOL, Tokyo, Japan) were utilized to evaluate the purity of the elements. The crystalline structure of the ZnO nanoparticles was evaluated using XRD. X-ray diffraction used to assess the crystallization and phasing purity of ZnO nanoparticles (XRD Modelle-D8 Advance, Bruker, Germany). The Malvern Zetasizer Nanosystem (Worcestershire, U.K.) was used to assess the hydrodynamic diameter and zeta potential of the *Lactobacillus* mediated ZnO nanoparticles (ZnO NPs-Lb). To ensure uniform dispersion, the synthesized ZnO NPs-Lb were first dissolved in an aqueous solution and then filtered *via* a 0.22 µm syringe-driven filter unit. Using the DLS approach, the size distribution of the ZnO NPs-Lb was then ascertained using a compact scattering spectrometer from the Malvern Zetasizer Nano series [22].

Lactobacillus mediated ZnO NPs anticancer properties against a human cancer cell line

Cell cultures: Human lung cancer cells (A549) were obtained from the National Centre for Cell Sciences (NCCS), Pune, India. These cells were grown in Dulbecco's Modified Eagle Medium (DMEM), which was supplemented with a few vital elements, such as fetal bovine serum, sodium carbonate, sodium pyruvate, balanced salt solution (BSS), l-glutamine, glucose and non-essential amino acids. The medium was

carefully prepared to ensure the best conditions for cell growth and maintenance. A concentration of 100 IU/100 µg per mL was also added for penicillin and streptomycin. The cells were maintained at 37 ºC within a humidified, CO_2-enriched environment to promote ideal growth conditions [23].

Cytotoxicity evaluation: An MTT assay was performed to ascertain the inhibitory concentration (IC_{50}) value. A549 lung cancer cells were placed in a 96-well plate at a density of 1×10^4 cells per well and permitted to grow for 48 h until they reached around 80% confluence. A new medium was introduced, incorporating serial dilutions of ZnO NPs-Lb. The cells underwent incubation for further 48 h. Subsequently, the medium was removed and 100 µL of MTT solution was introduced into each well, followed by incubation at 37 ºC for 4 h. Following the removal of the supernatant, 50 µL of DMSO was introduced to each well to facilitate the dissolution of the formazan crystals, which was then incubated for 10 min. The measurement of optical density (OD) was conducted at a wavelength of 620 nm by Thermo-Multiskan EX ELISA plate reader [24]. The optical density values were subsequently utilized to determine the percentages of cell viability through a formula:

$$\text{Viability (\%)} = \frac{\text{OD value of experimental sample}}{\text{OD value of experimental control}} \times 100$$

Morphological study: The density of the human cancer cells chosen for the experiment was 1×10^5 cells per coverslip. The subjects were exposed to ZnO NPs-Lb at varying concentrations (10 µg/mL, 25 µg/mL, 50 µg/mL) for 24 h. Following this, the cells were fixed using a solution composed of ethanol and acetic acid in a 3:1 volume ratio. The coverslips were carefully arranged on glass slides to enable the morphometric analysis. The images were obtained from three monolayers in each experimental group. The morphological changes of the cells were examined using Nikon's bright field inverted light microscopy at 10X magnification [25].

Fluorescence microscopic analysis of apoptotic cell death: Acridine orange (AO) and ethidium bromide (EtBr) dye mixture diluted in 1 µL of distilled water and added to a suspension of cells on microscope coverslips. A549 lung cancer cells underwent treatment with varying concentrations of ZnO NPs-Lb nanoparticles. The cells were gathered, washed with phosphate-buffered saline (PBS, pH 7.2) and stained with the AO/EtBr dye mixture. Following 2 min of incubation, the cells underwent two washes with PBS and were subsequently analyzed using a fluorescence microscope (Nikon Eclipse, Inc., Japan) at a magnification of 400X, employing a 580 nm excitation filter. Cells were positioned on glass coverslips within six-well plates and exposed to different concentrations of ZnO NPs-Lb for a duration of 24 h. The cells underwent treatment with 0.2% Triton X-100 (50 µL) for a duration of 10 min at room temperature to facilitate permeabilization. About 10 µL of DAPI stain were applied, followed by the careful placement of a coverslip over the cells to ensure uniform staining. The cells were then analyzed using the Nikon Eclipse fluorescence microscope.

Cell cycle analysis: The selected A549 lung cell lines (2×10^5 cells/10 cm dishes) were treated with varying concentrations of the material for 24 h each. The cells were harvested using centrifugation, then washed with ice-cold PBS and were later resuspended in ice-cold 70% ethanol for overnight. The cells underwent treatment with 10 µg/mL of RNase at 37 ºC, subsequently subjected to centrifugation and stained with 40 µg/mL of propidium iodide (PI) for 30 min. The DNA content was subsequently assessed using flow cytometry on a BD FACS Verse, USA.

Apoptotic protein expression analysis: Western blotting was used to examine ZnO NPs-Lb on expression of apoptotic and anti-apoptotic proteins in treated and untreated cells. A549 cells (1.5×10^6) were cultivated in 100 mm dishes and exposed to varying concentrations of ZnO NPs-Lb for 24 h. Following the treatment, the medium was removed and the cells were subjected to multiple washes using phosphate-buffered saline (PBS). The cells were then lysed using 0.1 mL of lysis buffer per plate for approximately 20 min. This was followed by centrifugation to collect the supernatant, which served as the protein extract. Equal amounts of protein from each sample underwent separation on a 12% SDS-polyacrylamide gel through electrophoresis, followed by transfer to a nitrocellulose membrane. The membranes were treated to a blocking process with a 10% skimmed milk solution in water for 1 h, followed by washing with PBS containing 0.1% Tween-20. Primary antibodies specifically targeting p53, cytochrome c, Bcl-2 and β-actin were applied at a dilution of 1:1000 and incubation at 4 ºC. Unbound primary antibodies eliminated by washing, then secondary antibodies added and incubated at room temperature for 1 h. The visualization of protein bands was conducted to assess the expression levels.

Gene expression studies by semi-quantitative reverse transcriptase-polymerase chain reaction (qRT-PCR) in lung cancer cells: A549 human lung cancer cells were chemically treated and untreated control group were also created. Following a 24 h treatment period, the medium was completely removed from the flask. Isolation of total RNA was performed using TriZol reagent, which was subsequently followed by the reverse transcription of the RNA. The *c*DNA was extracted using the *c*DNA synthesis kit and then amplified according to the provided instructions. RT-PCR for apoptotic genes was performed using 20 µL of reaction mixture using random primer pairs (0.5 µL for forward and 0.5 µL for reverse). About 1.0 µL of 10X reaction buffer containing master mix (25 mM/l $MgCl_2$, 10 mM/l dNTPs, 2.5 U Taq polymerase), 10 µL of *c*DNA as template and the remaining volume consisting of 7 µL of nuclease-free deionized water. In a total of 32 amplification cycles, the primer underwent annealing at 55 ºC for 40 sec, followed by denaturation at 94 ºC for 1 min and extension at 72 ºC for 1 min. The final extension took place at 72 ºC for 10 min. Agarose gel electrophoresis was utilized to quantify the PCR products. Data analysis was conducted using Image J software and the intensity values were schematically represented using densitometry analysis.

Statistical analysis: All data were analyzed using analysis of variance (ANOVA). The results are presented as mean ± standard deviation. Statistical analysis was conducted with GraphPad Prism 5.0 (GraphPad Software, Inc.). A p-value of < 0.05 was considered to indicate a statistically significant difference.

RESULTS AND DISCUSSION

In this work, the synthesis procedure involves the bioreduction of zinc acetate with cell-free supernatant from the *Lactobacillus* sp., bacterial strain. Furthermore, UV-Vis, FTIR, XRD, SEM, TEM, EDX, zeta potential and DLS experiments were used to characterize the generated ZnO nanoparticles, confirming their nanoscale size and structural stability.

UV-visible spectral studies: The analysis using UV-visible spectroscopy showed a peak at approximately 380 nm, which suggests the formation of ZnO NPs. The evenness of the absorption band indicates a consistent distribution of the nanoparticles, serving as evidence of their stability and effective synthesis (Fig. 1). The absorbance spectrum of ZnO NPs-Lb was observed at 392 nm. According to Suba *et al*. [26], the absorption peak moved towards a shorter wavelength when compared to bulk ZnO, which has an absorption maximum at 379 nm.

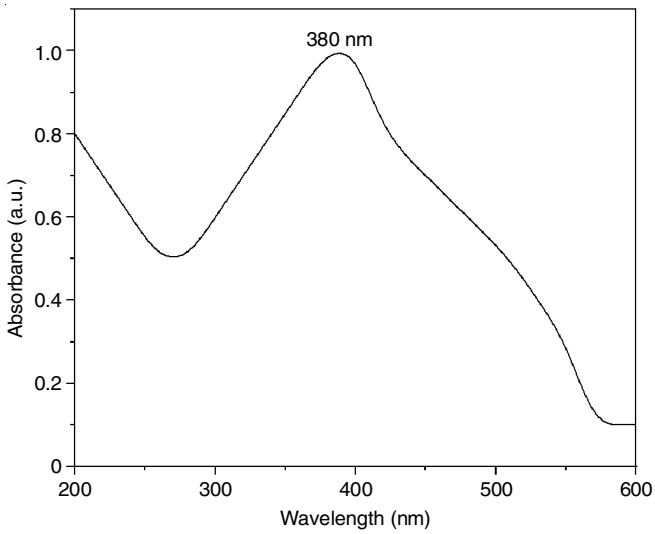

Fig. 1. UV-visible spectrum of *Lactobacillus* sp. mediated ZnO nanoparticles

FTIR studies: The transmittance spectra obtained through Fourier-transform infrared (FTIR) analysis of ZnO NPs-Lb revealed significant insights into the functional groups and molecular interactions that play a role in their formation. Fig. 2 illustrates that the FTIR spectra reveal clear bands spanning from 4000 to 500 cm^{-1}, which are associated with different chemical bonds and vibrational modes present in the nanoparticles. The significant peaks were identified at 2002.11 cm^{-1}, 1637.56 cm^{-1}, 1363.67 cm^{-1}, 1026.13 cm^{-1}, 866.04 cm^{-1}, 827.46 cm^{-1} and 690.52 cm^{-1}. These peaks suggest the presence of functional groups including hydroxyl, carboxyl and amine groups, along with the distinctive vibrations associated with ZnO bonds. The results indicate that bacterial metabolites play a role in the synthesis and stabilization of ZnO NPs.

The peak with a frequency of 2002.11 cm^{-1} indicates the presence of C≡C or C≡N stretching, which is indicative of alkyne or nitrile groups originating from bacterial metabolites [27,28]. The peak at 1637.56 cm^{-1} corresponds to the stretching of C=O bonds from amides or carboxyl groups. These groups are coordinated with proteins or organic acids that act as stabilizing agents [29]. In addition, the existence of alcohol, ester

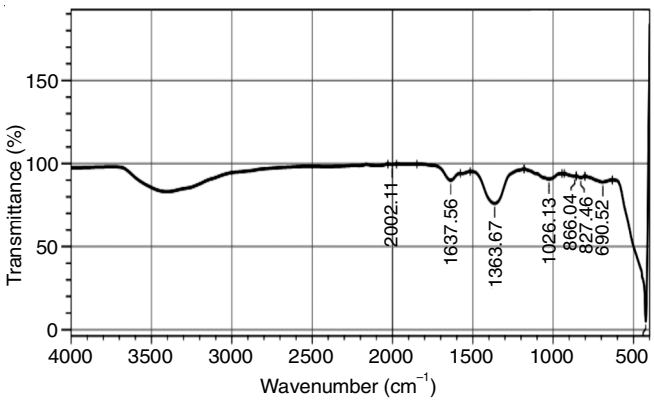

Fig. 2. FTIR spectrum of *Lactobacillus* sp. mediated ZnO nanoparticles

or ether groups can be inferred from the C-H bending frequency of 1363.67 cm^{-1} and the C-O stretching frequency of 1035.77 cm^{-1} [30]. At 866.04 and 827.46 cm^{-1}, there are peaks that correspond to the bending vibrations of aromatic rings, which are most likely caused by byproducts of bacterial metabolism. Recent study reported that the peak at 690.52 cm^{-1} is a confirmation of the Zn-O bond, which in turn verifies the successful synthesis of ZnO nanoparticles. The results of this study indicate that bacterial metabolites play a substantial role in the process of reducing, stabilizing and functionalizing ZnO nanoparticles. This serves to highlight the biocompatibility of these nanoparticles as well as their possible biological origin [31,32].

X-ray diffraction studies: The X-ray diffraction (XRD) analysis on ZnO NPs-Lb validated their phase and crystalline structure, displaying a distinct diffraction pattern characteristic of a hexagonal wurtzite structure. The significant peaks were identified at particular 2θ values, aligning with the crystallographic planes (*hkl*): (100), (002), (101), (102), (110), (103), (200), (112), (201), (004) and (202) (Fig. 3). The observed peaks reflect the clearly defined crystalline characteristics of the ZnO NPs-Lb, affirming their successful synthesis and offering valuable insights into their structural integrity. The results of this study were in agreement with the reference data obtained from the Joint Committee on Powder Diffraction Standards (JCPDS card No. 79–2205), which indicated that the green synthesized ZnO nanoparticles possessed a high degree of crystallinity and purity. These results are also matched with the reported works [33,34].

SEM studies: The analysis conducted through scanning electron microscopy (SEM) on ZnO NPs-Lb synthesized demonstrated that the nanoparticles were primarily spherical in shape, measuring between 30 and 40 nm, as illustrated in Fig. 4. The SEM images demonstrated a significant agglomeration, a characteristic often observed in the biosynthesized ZnO nanoparticles. The clustering observed can be ascribed to the elevated surface energy of the particles and the interactions between them, which are characteristic of nanoparticles produced *via* biological techniques. Selvarajan & Mohanasrinivasan [35] explored the intracellular production of pure crystalline and spherical ZnO NPs, which varied in size from 7 to 19 nm, derived from *Lactobacillus plantarum* VITES07. The synthesized nanoparticles exhibited moderate stability, suggesting that the biomolecules

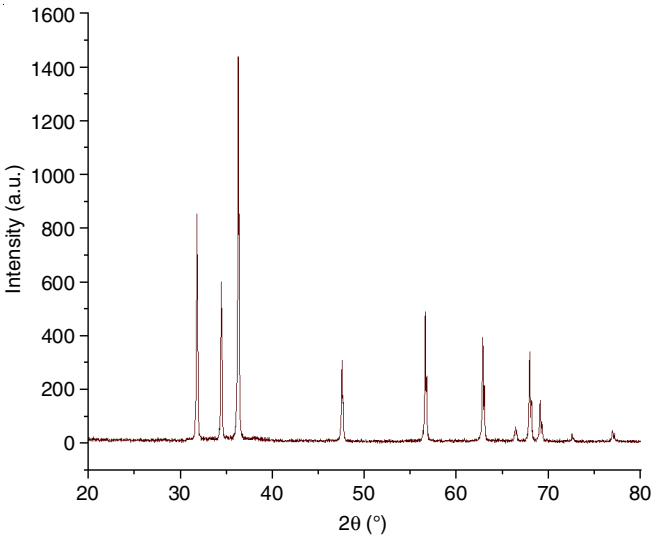

Fig. 3. XRD spectrum of *Lactobacillus* sp. mediated ZnO nanoparticles

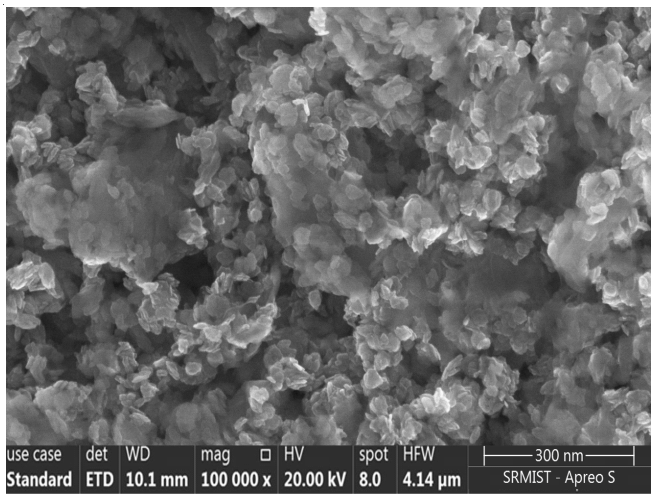

Fig. 4. Scanning electron microscopic image of *Lactobacillus* sp. mediated ZnO nanoparticles

released by the bacterial strain functioned as a capping agent during the synthesis process. Furthermore, spherical ZnO NPs measuring between 100 and 130 nm were synthesized using *Rhodococcus pyridinivorans* along with zinc sulphate as a substrate [36].

TEM studies: The size and surface morphology of ZnO NPs-Lb were examined through transmission electron microscopy (TEM), as illustrated in Fig. 5. The TEM images demonstrated that the ZnO nanoparticles, facilitated by the genus *Lactobacillus*, exhibited sizes varying from 30 nm to 43 nm. The grey coloured nanoparticles had a spherical morphology and were uniformly distributed indicating the presence of bioactive components from the probiotic compounds that serve as stabilizers. The findings indicate that the supernatant from *Lactobacillus* sp., effectively promoted the formation of ZnO nanoparticles while also acting as a capping agent. The bioactive components present in the supernatant were instrumental in the reduction of zinc ions, while the capping effect contributed to the prevention of agglomeration, thereby maintaining the stability of the ZnO nanoparticles. The TEM and SAED images

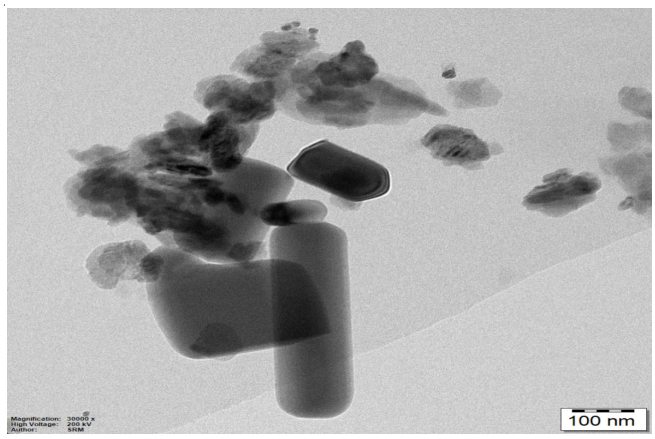

Fig. 5. Transmission electron microscopic image of *Lactobacillus* sp. mediated ZnO nanoparticles

confirmed the development of crystalline metal nanostructures, providing further understanding of the spherical morphology and dimensional characteristics of the metal nanoparticles [37].

EDX studies: Investigation was carried out to identify and quantify the components found in ZnO NPs-Lb. The EDX analysis results indicated the presence of zinc (Zn) and oxygen (O) atoms in the ZnO nanoparticles, as illustrated in Fig. 6. This provided a better knowledge of the elemental composition of ZnO nanoparticles and confirmed their successful formation [38].

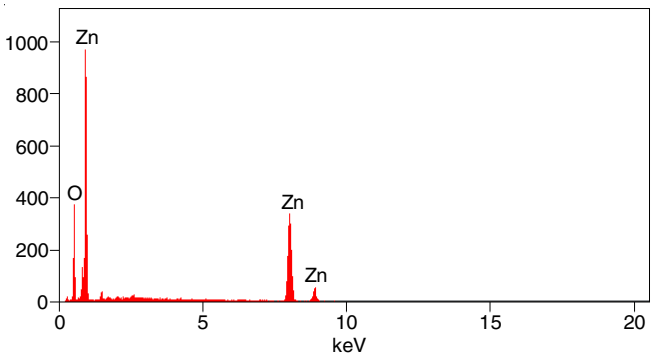

Fig. 6. Energy dispersive X-ray spectrum of *Lactobacillus* sp. mediated ZnO nanoparticles

Zeta potential: The ZnO NPs that were biosynthesized demonstrated significant electrostatic repulsive forces, effectively helping in the prevention of agglomeration. The nanoparticles exhibited a high positive zeta potential of 14.2 mV (Fig. 7), display remarkable stability, which suggests their capacity to maintain a well-dispersed state and resist aggregation. The electrostatic repulsion force inhibits the aggregation of nanoparticles with strong negative or positive zeta potential, while particles with low zeta potential are more likely to aggregate [35]. The significant positive potential value of the synthesized ZnO NPs suggests their high stability and strong cationic characteristics. Due to the influence of electrostatic attraction, nanoparticles with a positive charge demonstrated a stronger adherence to the negatively charged surfaces of cell membranes. This interaction facilitated the entry of ZnO nanoparticles into cells, subsequently enhancing their toxicity towards microorg-

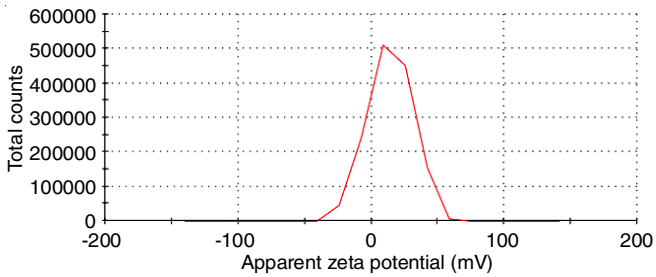

Fig. 7. Zeta potential analysis of *Lactobacillus* mediated ZnO nanoparticles

anisms. Inside the cells, they accumulated and disrupted the normal function of the cancer cells, leading to toxicity [39].

Particle size and distribution (DLS): The analysis of ZnO NPs-Lb using DLS indicated a Z-average size of 614.2 nm, accompanied by a polydispersity index (PDI) of 0.325. Fig. 8 presents the DLS distribution. The International Organization for Standardization (ISO) states that PDI values exceeding 0.7 reflect a wide size distribution, whereas PDI values under 0.5 indicate a greater level of monodispersity. Consequently, the PDI value of 0.325 suggests that the ZnO nanoparticles possess a narrow size distribution, indicating a greater uniformity in particle size. In a technical sense, the size of the nanoparticles that were measured using DLS was calculated from the metal core of the nanoparticles to the layer that surrounded the nanoparticles [40]. Due to this calculation, the size of the nanoparticles was found to be increased.

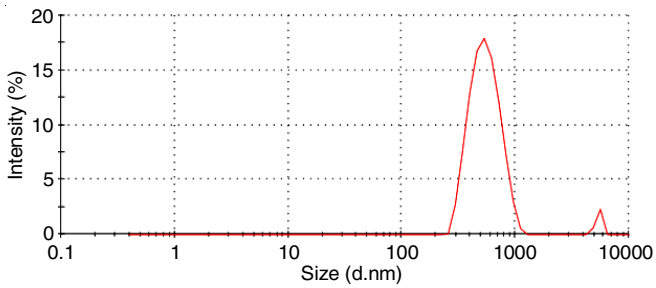

Fig. 8. DLS analysis of *Lactobacillus* sp. mediated ZnO nanoparticles

Anticancer activity: An experiment was conducted to explore the impact of ZnO NPs-Lb on the lung cancer cells. The A549 lung cancer cells underwent exposure to different concentrations of ZnO NPs-Lb, reaching up to 100 µg/mL, over a duration of 24 h. The MTT assay was employed to evaluate cytotoxic effects. The findings indicated that ZnO NPs-Lb effectively suppressed cell proliferation, with the extent of suppression correlating with the dosage applied. Fig. 9 showed that the ZnO NPs-Lb significantly inhibited the proliferation of lung cancer cells, demonstrating an IC_{50} value of 38 ± 1.5 µg/mL. In contrast, cisplatin, exhibited an IC_{50} value of 19 ± 0.5 µg/mL in A549 lung cancer cells. These findings display an impressive effectiveness of ZnO nanoparticles synthesized by the genus *Lactobacillus* in specifically targeting cancer cells, suggesting a possible alternative to traditional cancer therapies. Multiple studies have shown that ZnO nanoparticles can specifically target cancer cells while sparing normal cells, highlighting their promising potential for therapeutic use. The cancer cells typically exhibit a greater negative charge on their surface

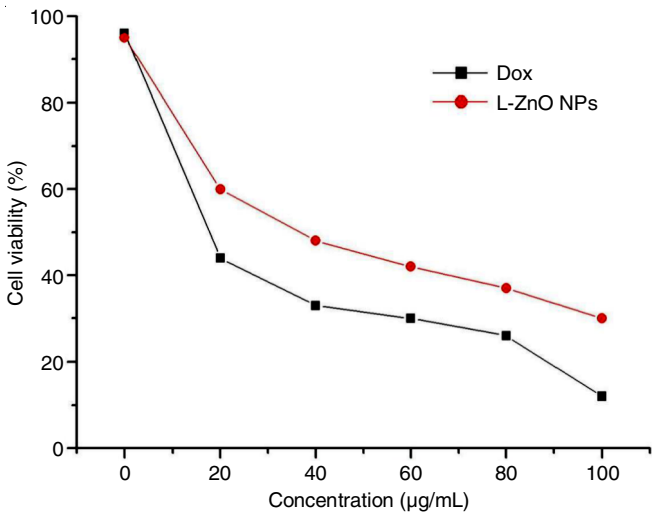

Fig. 9. MTT analysis of *Lactobacillus* sp. mediated ZnO nanoparticles (lung cancer cells A549)

compared to normal cells. ZnO nanoparticles, especially the positively charged ones, show enhanced adhesion to the negatively charged membranes of cancer cells, which promotes their effective absorption.

Recently, the green-synthesized ZnO NPs using *Luffa acutangula* peel extract with a size range of 10-20 nm were evaluated for their effectiveness against human cancer cell lines Huh-7 and MCF-7. The IC_{50} values for these ZnO NPs were found to be 40 µg/mL and 121 µg/mL, respectively [41]. It is evident that the present findings are encouraging in comparison to those reported studies. For example, the ZnO NPs that were synthesized from *Rapanus sativus*, demonstrated an IC_{50} value of 40 µg/mL when tested against the A549 cell line as reported by Umamaheswari *et al.* [42]. Moreover, it was observed that the viability of cell line reduced as the concentration of nanoparticles and conventional drugs increased, because they pose lower risks compared to chemically synthesized ZnO NPs [43, 44].

Morphological studies: The A549 lung cancer cells were exposed to the IC_{50} concentration of ZnO nanoparticles synthesized by using *Lactobacillus* sp. for 24 h, resulting in significant morphological changes.. The cells that were treated showed significant changes in their appearance, with the extent of these changes depending on the concentration of the nanoparticles used (Fig. 10). As the concentration of ZnO NPs-Lb increased, cytotoxicity correspondingly increased. The treatment resulted in cellular shrinkage, membrane blebbing, reorganization and a decrease in the overall number of viable cells. The findings indicated that ZnO NPs-Lb have prompted apoptosis in A549 lung cancer cells, as shown in Fig. 10b-d. The untreated control cells exhibited no significant morphological alterations or adverse effects, as showed in Fig. 10a.

The biosynthesized ZnO nanoparticles can disrupt cellular membranes, induce vacuole formation and alter the metabolic processes of cancer cells, hence activating the apoptosis pathway and resulting in the effective elimination of cancer cells. Alongside the alterations in cellular and nuclear structure, the introduction of ZnO NPs results in the liberation of intracellular

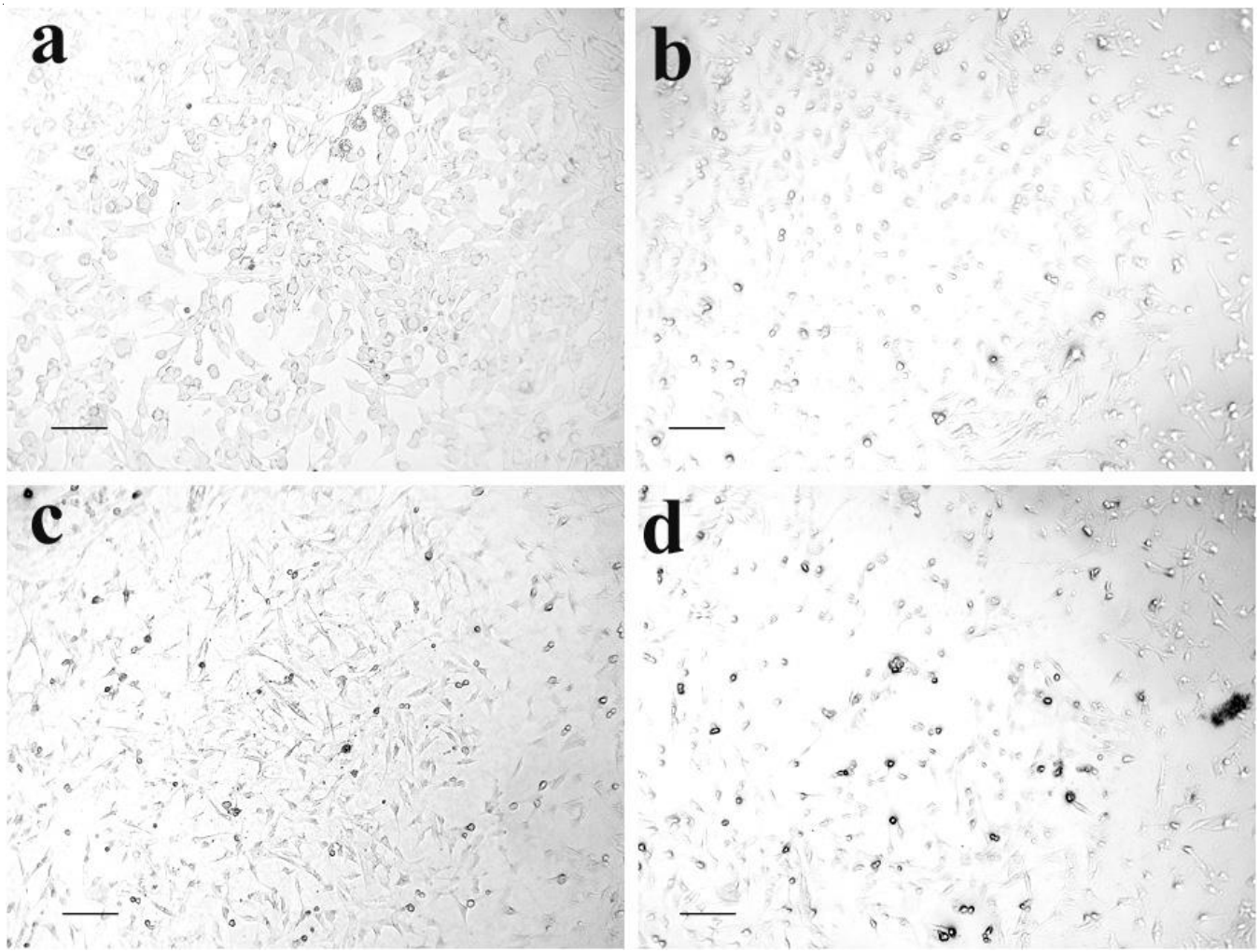

Fig. 10. Morphological analysis of *Lactobacillus* sp. mediated ZnO nanoparticles-treated A549 cells for 24 h (a) control, (b)10 µg/mL, (c) 25 µg/mL and (d) 50 µg/mL

zinc ions, which in turn promotes the generation of reactive oxygen species (ROS) [45]. Microbe mediated ZnO NPs are attracting significant attention as promising anticancer therapeutic candidates with lower toxicity compared to chemically synthesized ZnO NPs [44].

Fluorescence microscopic analysis: AO/EtBr and DAPI staining for nuclear fragmentation: The study explored the apoptotic effects of ZnO NPs-Lb on lung cancer A549 cells through fluorescence microscopy techniques. The cells were treated with a specified dose of nanoparticles, and apoptotic activation was assessed by acridine orange/ethidium bromide (AO/EtBr) staining. Fluorescence microscopy demonstrated that live cells displayed a vivid green fluorescence, whereas the dead cells showed a unique acridine orange fluorescence.

Fig. 11a shows a standard representation of viable cell abundance in the untreated control group. Conversely, A549 lung cancer cells exposed to ZnO NPs-Lb exhibited a significant rise in apoptotic cells, accompanied by the development of apoptotic bodies. The apoptotic cells exhibited features such as nuclear shrinkage, nuclear damage and the development of blebs, which displayed an orange/red fluorescence (Fig. 11b-d). The results indicate that the treatment led to remarkable apoptotic alterations in the A549 lung cancer cells, highlighting the promise of *Lactobacillus* mediated ZnO nanoparticles as a potential apoptosis inducer in cancer cells.

We additionally evaluated the efficacy of ZnO NPs-Lb using DAPI staining. Fig. 12 displays fluorescence microscopic pictures of cells labelled with DAPI following 24 h of treatment, both in the presence and absence of ZnO NPs-Lb. The cells subjected to the nanoparticles displayed unique properties. In A549 lung cancer cells, bright patches were observed, signifying aggregated chromatin and fragmented nuclei (Fig. 12b-d). The untreated control cells (Fig. 12a) exhibited no notable changes. The fluorescence microscopic examination unequivocally indicates that ZnO NPs-Lb possess considerable potential as a therapeutic agent in cancer treatment. The results of study indicate a significant inhibition of proliferation in the A549 lung cancer cell line as a consequence of treatment with ZnO NPs-Lb. The results are consistent with earlier studies investigating the effects of nanoparticles on cell death across different cell types [46,47].

Effect of *Lactobacillus* mediated ZnO nanoparticles on cell cycle arrest by flow cytometry: The analysis of cell cycle in PI-stained cells demonstrated that ZnO NPs-Lb caused

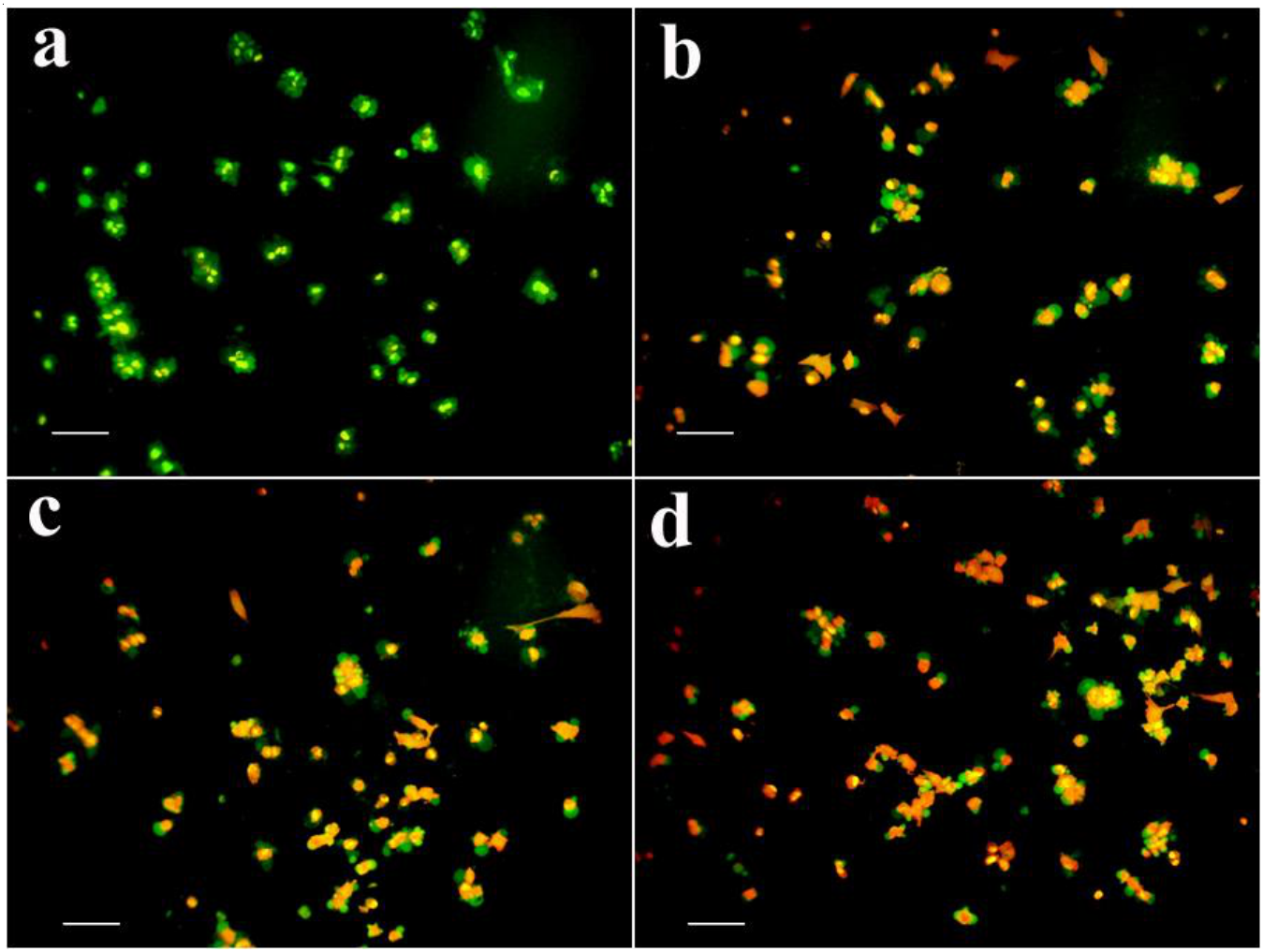

Fig. 11. AO/EtBr staining assay of *Lactobacillus* sp. mediated ZnO nanoparticles treated lung cancer A549 cells (a) control, (b) 10 µg/mL, (c) 25 µg/mL and (d) 50 µg/mL

cell cycle arrest specifically at the S phase. Fig. 13 shows that the treatment with ZnO nanoparticles had a significant effect on the progression of cells through different phases of the cell cycle. The untreated control exhibited a rise in cell numbers across the G0-G1, S and G2/M phases, suggesting a significant level of active cell proliferation. However, following treatment with ZnO NPs-Lb nanoparticles, a significant alteration was observed in the cell cycle distribution. The increase in the proportion of cells in the G0/G1 phase indicates a potential obstruction in the progression from G0/G1 to the S phase. The distribution of cells in the S phase, which is responsible for DNA replication, was significantly reduced when compared to the control group. The findings indicate that the ZnO NPs-Lb primarily exert their inhibitory effects on proliferation by inducing cell cycle arrest during the DNA replication phase. The findings demonstrated that the nanoparticles obstructed the natural advancement of the cell cycle, specifically interfering with DNA synthesis, which ultimately leads to the reduced proliferation of lung cancer A549 cells.

Zhang *et al*. [48] reported that the G2/M phase arrest of the cell cycle can inhibit growth and cause death by preventing damaged chromosomes from separating during mitosis. This is the mechanism by which the cell cycle is halted. According to the findings of a previous investigation, the overexpression of UBQLN4 led to an increase in the proportion of GES-1 cells that were in the G2/M phase in compared to the control cells. According to Huang *et al*. [49], this detection increases the possibility that the apoptotic program was launched by a halt in the transition from the G2/M state to the M state. Previously investigated that the capacity of sitosterol-fabricated chitosan nanocomplexes to induce cell cycle arrest is the principal factor responsible for their cell-inhibiting properties [50]. Moreover, the present findings align with those of Namvar *et al*. [51], who demonstrated that iron oxide nanoparticles can induce cell cycle arrest and apoptosis in MCF-7, HepG2 and Jurkat cells.

Western blot analysis: The apoptotic signaling pathway consists of a significant array of molecules that are intricately linked together. For the purpose of determining the mechanism of apoptosis that was activated by the ZnO NPs-Lb in the lung cancer A549 cells, a western blot analysis was performed to detect a wide variety of apoptotic characteristics (Fig. 14). It is important to observe that the expression of apoptotic proteins including p53 and cytochrome c was found to be upregulated, whereas the expression of Bcl-2, which is an anti-apoptotic

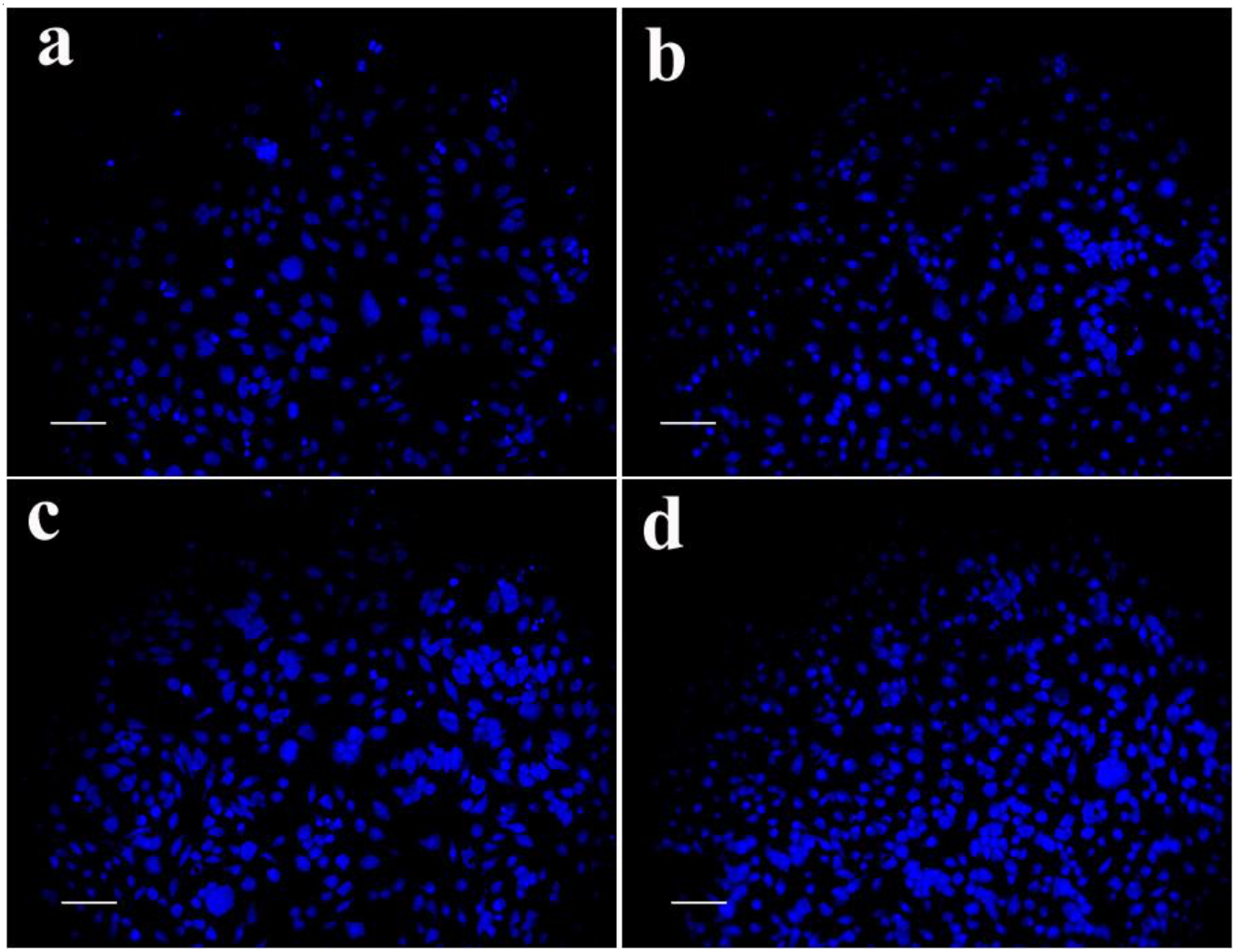

Fig. 12. DAPI staining assay of *Lactobacillus* sp. mediated ZnO nanoparticles treated lung cancer A549 cells (a) control, (b) 10 µg/mL, (c) 25 µg/mL and (d) 50 µg/mL

protein, was shown to be downregulated throughout the experiment. The present findings align with the process indicating that the reduction or inhibition of anti-apoptotic proteins can induce mitotic distress, DNA damage and ultimately, cell death.

The anti-apoptotic action of Bcl-2 can be effectively counteracted by the presence of apoptotic protein of critical importance. Similarly study by Zhang *et al*. [48], overexpression of Bcl-2 impedes caspase activation and diminishes the release of cytochrome C from the mitochondria to the cytoplasm in the intrinsic apoptotic pathway mediated by mitochondria. ZnO nanoparticles produced from *Solanum procumbens* have demonstrated efficacy in impairing lung cancer cells. During the initial phases of apoptosis, less resilient cells experienced both survival and demise. Upon adjusting the dosage to a moderate level, a reduction in the number of viable cells was observed; however, there was no significant impact on the incidence of early or late apoptosis [52]. These data demonstrate that ZnO NPs-Lb largely promote cell death *via* apoptosis.

Semi-quantitative RT-PCR analysis for apoptotic gene expression: This investigation involved analyzing the expression of apoptotic genes in cancer cells subjected to different concentrations of ZnO NPs-Lb over a 48 h period, utilizing semi-quantitative RT-PCR for assessment. The expression profiles of essential genes associated with apoptosis, such as p53, cytochrome c, Bcl-2 and β-actin (serving as a housekeeping gene), were analyzed. The findings indicated that the A549 lung cancer cells treated with ZnO NPs-Lb showed markedly elevated expression levels of these genes in comparison to the control cells that were not exposed (Fig. 15). In particular, cells that were treated with ZnO NPs-Lb exhibited a 2-3 fold enhancement in the expression levels of p53, cytochrome c and Bcl-2 genes when compared to the control groups across different exposure concentrations. The agarose gel electrophoresis image of the RT-PCR products (Fig. 15) provides additional confirmation of these findings, displaying clear and amplified bands that correlate with the elevated gene expression observed in the treated cells. The findings indicate that ZnO NPs-Lb could enhance apoptosis in lung cancer A549 cells by increasing the expression of pro-apoptotic genes such as p53 and cytochrome c, while also influencing the expression of anti-apoptotic genes like Bcl-2. The gene expression profile supports the suggested mechanism by which the nanoparticles trigger apoptotic signalling pathways, thereby playing a role in the suppression of cancer cell growth.

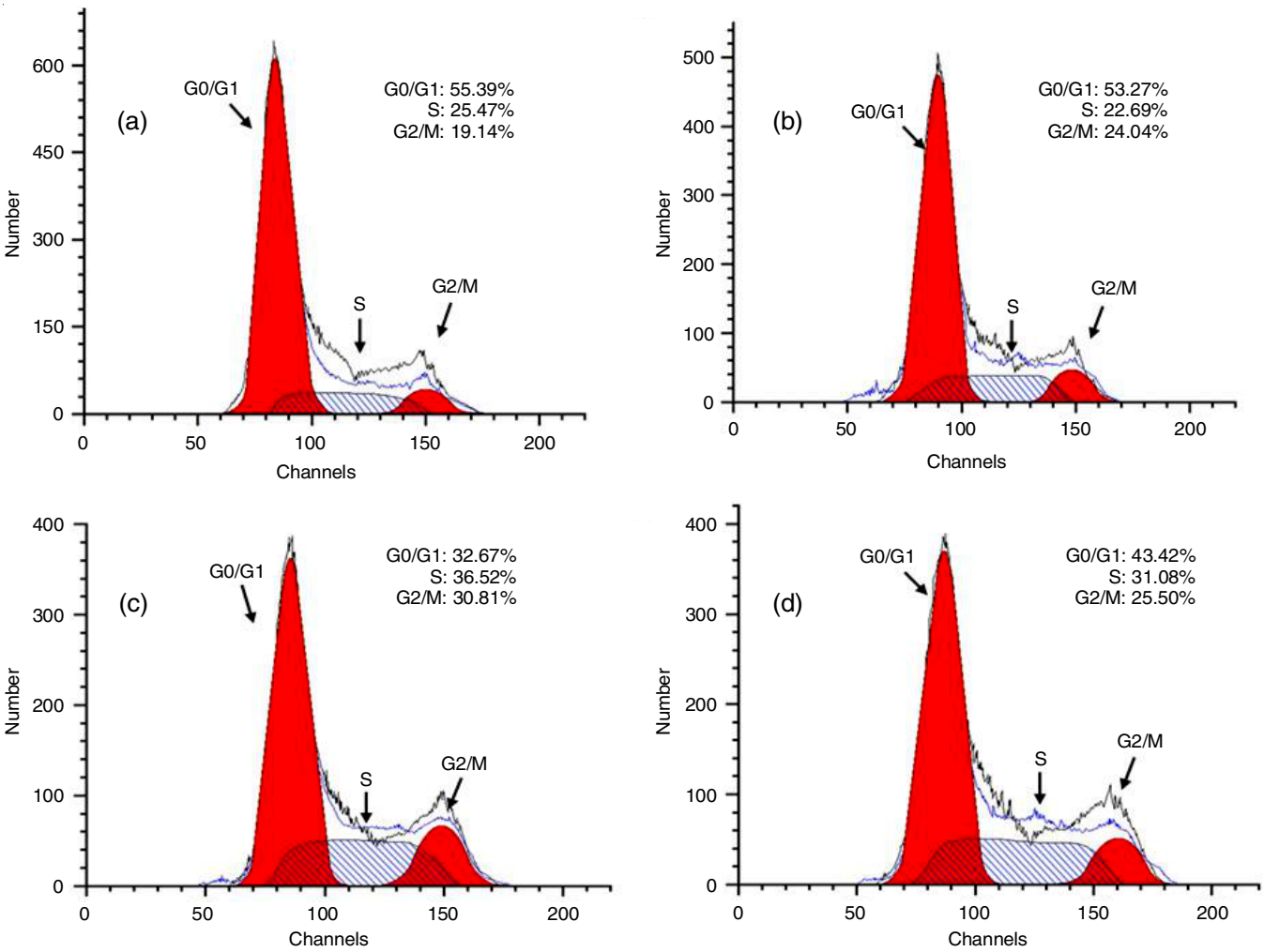

Fig. 13. Induction of cell-cycle arrest through *Lactobacillus* sp. mediated ZnO nanoparticles treated lung cancer A549 cells (a) control (b) 10 µg/mL (c) 25 µg/mL and (d) 50 µg/mL

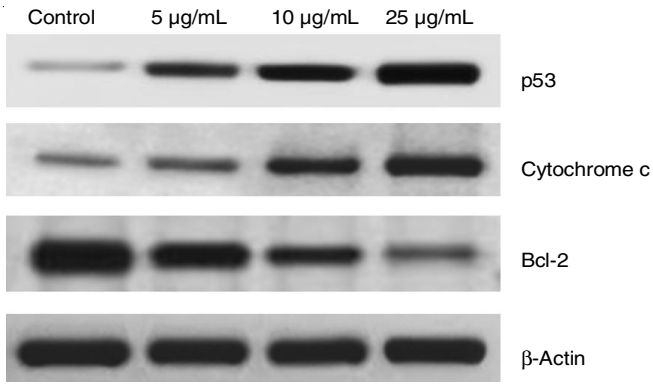

Fig. 14. Expression of apoptotic and anti-apoptotic proteins by western blot analysis in lung cancer A549 cells treated with *Lactobacillus* sp. mediated ZnO nanoparticles

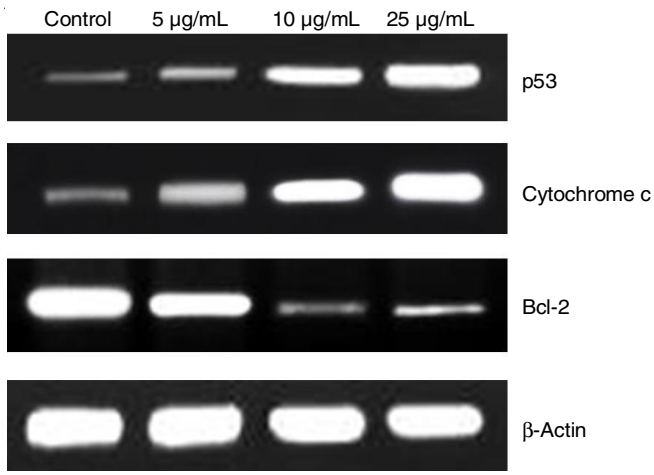

Fig. 15. Effect of *Lactobacillus* sp. mediated ZnO nanoparticles on the gene expression of apoptosis related genes

To determine the occurrence of apoptosis, DNA fragmentation assays were employed, alongside real-time polymerase chain reaction (RT-PCR) and western blotting methods to assess the expression changes of apoptotic genes, including caspase-3 and p53 [53], the results demonstrate that the nanoparticles generated *via* biosynthesis exhibited cytotoxic effects on the HeLa, MCF-7 and HCT-15 cell lines examined in this study. Recent reports indicate that mRNA expression levels of E-cadherin, Bax, caspase-3 and caspase-9 were elevated in cells treated with CS-LP-AgNPs, whereas the expression levels of N-cadherin, Snail and BCl2 were downregulated. This was compared to the expression levels observed in control cells [54].

Conclusion

This study reports investigates the synthesis of zinc oxide nanoparticles (ZnO NPs) facilitated by environmentally benign, non-toxic probiotic strain of *Lactobacillus* sp., for use against A549 lung cancer cells. The novel methodology resulted in the synthesis of small, stable ZnO nanoparticles, which were characterized by many analytical techniques, including UV-Vis spectroscopy, FTIR, XRD, SEM, TEM, EDX, zeta potential and DLS analysis, thereby validating the efficacy of the biosynthetic process. The biosynthesized ZnO NPs-Lb had considerable anti-proliferative and apoptotic effects at low doses. Apoptosis induction was effectively validated using DAPI and acridine orange/ethidium bromide (AO/EB) double staining techniques. The results emphasized the significant apoptosis of A549 cells triggered by ZnO NPs-Lb. Apoptotic protein activation was recognized as a crucial element in the apoptosis process, resulting in DNA damage and nuclear condensation. These data indicate that ZnO NPs-Lb may activate the apoptotic pathway, resulting in the killing of cancer cells. The study further illustrates the safety and promise of ZnO NPs-Lb for biomedical applications, especially in cancer therapy.

ACKNOWLEDGEMENTS

The authors sincerely acknowledge the financial support provided by the DBT Star College Scheme and DST-FIST, Government of India, for strengthening the laboratory infrastructure and fostering research and development, which has been instrumental in advancing our research work.

CONFLICT OF INTEREST

The authors declare that there is no conflict of interests regarding the publication of this article.

REFERENCES

1. R.L. Siegel, K.D. Miller, N.S. Wagle and A. Jemal, *CA* Cancer, *J. Clin.*, **73**, 17 (2023); https://doi.org/10.3322/caac.21763
2. A.M. Wolf, K.C. Oeffinger, T.Y.C. Shih, L.C. Walter, T.R. Church, E.T. Fontham, E.B. Elkin, R.D. Etzioni, C.E. Guerra, R.B. Perkins, K.K. Kondo, T.B. Kratzer, D. Manassaram-Baptiste, W.L. Dahut and R.A. Smith, *CA Cancer J. Clin.*, **74**, 50 (2024); https://doi.org/10.3322/caac.21811
3. A.K. Ganti, A.B. Klein, I. Cotarla, B. Seal and E. Chou, *JAMA Oncol.*, **7**, 1824 (2021); https://doi.org/10.1001/jamaoncol.2021.4932
4. M. Pirooznia, X. Wu, J.N. Bella, F. Zhang and D. Jovanovic, *Front. Genet.*, **15**, 1369247 (2024); https://doi.org/10.3389/fgene.2024.1369247
5. J. Sarkar, M. Ghosh, A. Mukherjee, D. Chattopadhyay and K. Acharya, *Bioprocess Biosyst. Eng.*, **37**, 165 (2014); https://doi.org/10.1007/s00449-013-0982-7
6. M.H. Kalaba, G.M. El-Sherbiny, E.A. Ewais, O.M. Darwesh and S.A. Moghannem, *BMC Microbiol.*, **24**, 254 (2024); https://doi.org/10.1186/s12866-024-03392-4
7. G. Bisht, S. Rayamajhi, B. Kc, S.N. Paudel, D. Karna and B.G. Shrestha, *Nanoscale Res. Lett.*, **11**, 537 (2016); https://doi.org/10.1186/s11671-016-1734-9
8. Z. Alhalili, *Molecules*, **28**, 3086 (2023); https://doi.org/10.3390/molecules28073086
9. M. Bundschuh, J. Filser, S. Lüderwald, M.S. McKee, G. Metreveli, G.E. Schaumann, R. Schulz and S. Wagner, *Environ. Sci. Eur.*, **30**, 6 (2018); https://doi.org/10.1186/s12302-018-0132-6
10. R.A. de Jesus, G.C. de Assis, R.J. Oliveira, J.A.S. Costa, C.M.P. da Silva, H.M.N. Iqbal and L.F.R. Ferreira, *Nano-Struct. Nano-Objects*, **37**, 101071 (2024); https://doi.org/10.1016/j.nanoso.2023.101071
11. M. Anbuvannan, M. Ramesh, G. Viruthagiri, N. Shanmugam and N. Kannadasan, *Spectrochim. Acta A Mol. Biomol. Spectrosc.*, **143**, 304 (2015); https://doi.org/10.1016/j.saa.2015.01.124
12. H. Mohd Yusof, R. Mohamad, U.H. Zaidan and N.A. Abdul Rahman, *J. Anim. Sci. Biotechnol.*, **10**, 57 (2019); https://doi.org/10.1186/s40104-019-0368-z
13. B. Balraj, N. Senthilkumar, C. Siva, R. Krithikadevi, A. Julie, I.V. Potheher and M. Arulmozhi, *Res. Chem. Intermed.*, **43**, 2367 (2017); https://doi.org/10.1007/s11164-016-2766-6
14. S. Liang, C. Wang, Y. Shao, Y. Wang, D. Xing and Z. Geng, *Front. Bioeng. Biotechnol.*, **10**, 1026248 (2022); https://doi.org/10.3389/fbioe.2022.1026248
15. S. Anjum, M. Hashim, S.A. Malik, M. Khan, J.M. Lorenzo, B.H. Abbasi and C. Hano, *Cancers*, **13**, 4570 (2021); https://doi.org/10.3390/cancers13184570
16. R. Shanmugam, T. Munusamy, S. Jayakodi, K.A. Al-Ghanim, M. Nicoletti, N. Sachivkina and M. Govindarajan, *Fermentation*, **9**, 413 (2023); https://doi.org/10.3390/fermentation9050413
17. M. Murali, H.G. Gowtham, N. Shilpa, S.B. Singh, M. Aiyaz, R.Z. Sayyed, C. Shivamallu, R.R. Achar, E. Silina, V. Stupin, N. Manturova, A.A. Shati, M.Y. Alfaifi, S.E.I. Elbehairi and S.P. Kollur, *Front. Microbiol.*, **14**, 1227951 (2023); https://doi.org/10.3389/fmicb.2023.1227951
18. G. Hamad, R.A. Ombarak, M. Eskander, T. Mehany, F.R. Anees, R.A. Elfayoumy, S.A. Omar, J.M. Lorenzo and S.A.-E. Abou-Alella, *Lebensm. Wiss. Technol.*, **163**, 113603 (2022); https://doi.org/10.1016/j.lwt.2022.113603
19. A. Latif, A. Shehzad, S. Niazi, A. Zahid, W. Ashraf, M.W. Iqbal, A. Rehman, T. Riaz, R.M. Aadil, I.M. Khan, F. Özogul, J.M. Rocha, T. Esatbeyoglu and S.A. Korma, *Front. Microbiol.*, **14**, 1216674 (2023); https://doi.org/10.3389/fmicb.2023.1216674
20. S. Samanta, *Anticancer. Agents Med. Chem.*, **22**, 605 (2022); https://doi.org/10.2174/1871520621999201210220442
21. A.-Q. Yu and L. Li, *Nutr. Cancer*, **68**, 535 (2016); https://doi.org/10.1080/01635581.2016.1158300
22. A.S. Abdelbaky, T.A. Abd El-Mageed, A.O. Babalghith, S. Selim and A.M. Mohamed, *Antioxidants*, **11**, 1444 (2022); https://doi.org/10.3390/antiox11081444
23. Z.V. Mohammed Hussain and S.K. Sivanandhan, *Indian J. Pharm. Educ. Res.*, **55**, 566 (2021); https://doi.org/10.5530/ijper.55.2.95
24. S.Z.A. Khader, S.S.Z. Ahmed, M.R. Mahboob, S.B. Prabaharan, S.O. Lakshmanan, K.R. Kumar and D. David, *Braz. J. Pharm. Sci.*, **58**, e18594 (2022); https://doi.org/10.1590/s2175-97902022e18594
25. H. Subramaniam, C.K. Lim, L.H. Tey, L.S. Wong and S. Djearamane, *Sci. Rep.*, **14**, 30198 (2024); https://doi.org/10.1038/s41598-024-81384-0
26. S. Suba, S. Vijayakumar, E. Vidhya, V.N. Punitha and M. Nilavukkarasi, *Sens. Int.*, **2**, 100104 (2021); https://doi.org/10.1016/j.sintl.2021.100104
27. F. Tai, S. Wang, B. Liang, Y. Li, J. Wu, C. Fan, X. Hu, H. Wang, R. He and W. Wang, *J. Nanobiotechnology*, **20**, 15 (2022); https://doi.org/10.1186/s12951-021-01222-7
28. S. Rawat, K. Samreen, A.K. Nayak, J. Singh and J.R. Koduru, *Environ. Nanotechnol. Monit. Manag.*, **15**, 100426 (2021); https://doi.org/10.1016/j.enmm.2021.100426
29. S. Vijayakumar, C. Krishnakumar, P. Arulmozhi, S. Mahadevan and N. Parameswari, *Microb. Pathog.*, **116**, 44 (2018); https://doi.org/10.1016/j.micpath.2018.01.003
30. V. Patel, C. Shah, M. Deshpande, and D. Madamwar, *Appl. Biochem. Biotechnol.*, **178**, 1630 (2016); https://doi.org/10.1007/s12010-015-1972-9

31. L. Zare, K. Namratha, M. S. Thakur, and K. Byrappa, *Mater. Res. Bull.*, **109**, 49 (2019); https://doi.org/10.1016/j.materresbull.2018.09.025
32. D. Kundu, C. Hazra, A. Chatterjee, A. Chaudhari and S. Mishra, *J. Photochem. Photobiol. B: Biol.*, **140**, 194 (2014); https://doi.org/10.1016/j.jphotobiol.2014.08.001
33. M.M. Shawki, M.M. Eltarahony and E.M. Moustafa, *Curr. Nanosci.*, **18**, 535 (2022); https://doi.org/10.2174/1573413717666211026151538
34. M. El-Khawaga, M..A. Elsayed, M. Gobara, A.A. Suliman, A.H. Hashem, A.A. Zaher, M. Mohsen and S.S. Salem, *Biomass Conv. Bioref.*, **15**, 2685 (2025); https://doi.org/10.1007/s13399-023-05131-7
35. E. Selvarajan and V. Mohanasrinivasan, *Mater. Lett.*, **112**, 180 (2013); https://doi.org/10.1016/j.matlet.2013.09.020
36. R.M. Tripathi, A.S. Bhadwal, R.K. Gupta, P. Singh, A. Shrivastav and B.R. Shrivastav, *J. Photochem. Photobiol. B*, **141**, 288 (2014); https://doi.org/10.1016/j.jphotobiol.2014.10.001
37. A. Mostafaei and A. Zolriasatein, *Prog. Nat. Sci.*, **22**, 273 (2012); https://doi.org/10.1016/j.pnsc.2012.07.002
38. D.K. Takci, M.S. Ozdenefe, T. Huner and H.A.M. Takci, *J. Aust. Ceram. Soc.*, (2024); https://doi.org/10.1007/s41779-024-01064-0
39. H. Agarwal, S. Menon, S.V. Kumar and S. Rajeshkumar, *Chem. Biol. Interact.*, **286**, 60 (2018); https://doi.org/10.1016/j.cbi.2018.03.008
40. H. Mohd Yusof, N.A. Abdul Rahman, R. Mohamad and U.H. Zaidan, *Appl. Sci.*, **10**, 6973 (2020); https://doi.org/10.3390/app10196973
41. R. Ananthalakshmi, S.R. Rathinam and A.M. Sadiq, *J. Inorg. Organomet. Polym. Mater.*, **31**, 1764 (2021); https://doi.org/10.1007/s10904-020-01852-8
42. A. Umamaheswari, S.L. Prabu, S.A. John and A. Puratchikody, *Biotechnol. Rep.*, **29**, e00595 (2021); https://doi.org/10.1016/j.btre.2021.e00595
43. S. Valsalam, P. Agastian, M.V. Arasu, N.A. Al-Dhabi, A.K. Ghilan, K. Kaviyarasu, B. Ravindran, S.W. Chang and S. Arokiyaraj, *J. Photochem. Photobiol. B*, **191**, 65 (2019); https://doi.org/10.1016/j.jphotobiol.2018.12.010
44. Y. Gao, M.A.V. Anand, V. Ramachandran, V. Karthikkumar, V. Shalini, S. Vijayalakshmi and D. Ernest, *J. Cluster Sci.*, **30**, 937 (2019); https://doi.org/10.1007/s10876-019-01551-6
45. G. Bisht and S. Rayamajhi, *Nanobiomedicine*, **3**, 63437 (2016); https://doi.org/10.5772/63437
46. H.K. Abdelhakim, E.R. El-Sayed and F.B. Rashidi, *J. Appl. Microbiol.*, **128**, 1634 (2020); https://doi.org/10.1111/jam.14581
47. B. Sumanth, T.R. Lakshmeesha, M.A. Alzohairy, A.C. Udayashankar, M.A. Ansari, B. Shobha, S.R. Niranjana, C. Srinivas and A. Almatroudi, *Int. J. Nanomedicine*, **15**, 8519 (2020); https://doi.org/10.2147/IJN.S271743
48. X.H. Zhang, Z.Q. Zou, C.W. Xu, Y.Z. Shen and D. Li, *Mol. Med. Rep.*, **4**, 273 (2011); https://doi.org/10.3892/mmr.2011.417
49. S. Huang, X. Dong, J. Wang, J. Ding, Y. Li, D. Li, H. Lin, W. Wang, M. Zhao, Q. Chang, N. Zhou, W. Cui and C. Huang, *Med. Sci. Monit.*, **24**, 3564 (2018); https://doi.org/10.12659/MSM.909621
50. K. Kavithaa, M. Paulpandi, S. Ramya, M. Ramesh, V. Balachandar, K. Ramasamy and A. Narayanasamy, *New J. Chem.*, **45**, 9251 (2021); https://doi.org/10.1039/D1NJ00913C
51. F. Namvar, R. Mohammad, J. Baharara, M. Mahdavi, E. Amini, S.K. Yeap, M.S. Chartrand and H.S. Rahman, *Int. J. Nanomedicine*, **9**, 2479 (2014); https://doi.org/10.2147/IJN.S59661
52. R. Wahab, M.A. Siddiqui, Q. Saquib, S. Dwivedi, J. Ahmad, J. Musarrat, A.A. Al-Khedhairy and H.S. Shin, *Colloids Surf. B Biointerfaces*, **117**, 267 (2014); https://doi.org/10.1016/j.colsurfb.2014.02.038
53. K.D. Datkhile, S.R. Patil, P.P. Durgawale, M.N. Patil, N.J. Jagdale, V.N. Deshmukh and A.L. More, *Nano Biomed. Eng.*, **12**, 241 (2020); https://doi.org/10.5101/nbe.v12i3.p241-252
54. A.K. Ravi, S. Muthukrishnan, G. Gunasangkaran, V.A. Arumugam, V. Shanmugam, K.M. Sakthivel, M.A. Pushpam and A. Kaliyaperumal, *Med. Microecology*, **22**, 100117 (2024); https://doi.org/10.1016/j.medmic.2024.100117